The Astrophysical Journal Letters, 893:L12 (6pp), 2020 April 10 https://doi.org/10.3847/2041-8213/ab8455

Dust Environment Model of the Interstellar Comet 2I/Borisov

G. Cremonese[1], M. Fulle[2], P. Cambianica[1], G. Munaretto[1,3], M. T. Capria[4], F. La Forgia[3], M. Lazzarin[3], A. Migliorini[4], W. Boschin[5,6,7], G. Milani[8], A. Aletti[9,8], G. Arlic[8], P. Bacci[10,8], R. Bacci[11,8], E. Bryssinck[12,8], D. Carosati[13,14,8], D. Castellano[8], L. Buzzi[9,8], S. Di Rubbo[8], M. Facchini[15,8], E. Guido[8], F. Kugel[16,8], R. Ligustri[8], M. Maestripieri[10,8], A. Mantero[17], J. Nicolas[8], P. Ochner[1,3], C. Perrella[8], R. Trabatti[18,8], and A. Valvasori[19,8]

[1] INAF—Osservatorio Astronomico, Vicolo Osservatorio 5, I-35122 Padova, Italy; gabriele.cremonese@inaf.it
[2] INAF—Osservatorio Astronomico, Via Tiepolo 11, I-34143 Trieste, Italy
[3] Dipartimento di Fisica e Astronomia, Universitá di Padova, vicolo Osservatorio 2, I-35122 Padova, Italy
[4] INAF—IAPS, Via del Fosso del Cavaliere 100, I-00133 Roma, Italy
[5] Fundación Galileo Galilei-INAF, Rambla José Ana Fernandez Pérez 7, E-38712 Breña Baja, TF, Spain
[6] Instituto de Astrofisica de Canarias, C/Via Lactea s/n, E-38205 La Laguna (Tenerife), Spain
[7] Departamento de Astrofisica, Univ. de La Laguna, Av. del Astrofisico Francisco Sánchez s/n, E-38205 La Laguna (Tenerife), Spain
[8] CARA Project, INAF—Osservatorio Astronomico, via Tiepolo 11, I-34143 Trieste, Italy
[9] Osservatorio G.V. Schiaparelli, Campo dei Fiori, I-21020 Varese VA, Italy
[10] Osservatorio Astronomico Montagna Pistoiese GAMP, Pian dei Termini, I-51028 San Marcello Pistoiese PT, Italy
[11] G. Pascoli Observatory, Castelvecchio Pascoli, Italy
[12] Brixiis Observatory, Kruibeke, Belgium
[13] EPT Observatories, Tijarafe, E-38780 La Palma, Spain
[14] INAF, TNG Fundacion Galileo Galilei, E-38712 La Palma, Spain
[15] Osservatorio Astronomico Geminiano Montanari, Cavezzo (MO), Italy
[16] Observatoire de Dauban, Banon 04, France
[17] Osservatorio Bernezzo, Bernezzo, Italy
[18] Stazione Astronomica Descartes, via Lambrinia 4, I-27013 Chignolo Po', Italy
[19] Osservatorio Felsina AAB, Via Varsellane, 12, I-40050 Monte San Pietro BO, Italy
Received 2020 February 24; revised 2020 March 25; accepted 2020 March 27; published 2020 April 10

Abstract

2I/Borisov is the first interstellar comet discovered on 2019 August 30, and it soon showed a coma and a dust tail. This study reports the results of images obtained at the Telescopio Nazionale Galileo telescope, on La Palma—Canary Islands, in 2019 November and December. The images have been obtained with the *R* filter in order to apply our dust tail model. The model has been applied to the comet 67P/Churyumov–Gerasimenko and compared to the Rosetta dust measurements showing a very good agreement. It has been applied to the comet 2I/Borisov, using almost the same parameters, obtaining a dust environment similar to that of 67P/Churyumov–Gerasimenko, suggesting that the activity may be very similar. The dust tail analysis provided a dust-loss rate $Q_d \approx 35\,\mathrm{kg\,s^{-1}}$ in 2019 November and $Q_d \approx 30\,\mathrm{kg\,s^{-1}}$ in 2019 December.

Unified Astronomy Thesaurus concepts: Planetary science (1255); Comets (280)

1. Introduction

The sudden appearance of the first interstellar object (ISO), 1I/2017 U1 (Oumuamua), in 2017 October was not completely unexpected. All the current planetary systems formation scenarios suggest that the interstellar space is filled with planetesimals, most of them icy, ejected by giant planets, as happened in the solar system (Engelhardt et al. 2017). More unexpected was instead the appearance of the second ISO in two years, 2I/2019 Q4 (Borisov) (hereafter 2I/Borisov), detected in 2019 August by the amateur Borisov, that challenged the assumed probability values of this kind of events. The real nature of 1I/Oumuamua is still under debate, even if the observations pointed at an asteroidal appearance, as no activity has been detected, despite the relatively large nongravitational effects (Micheli et al. 2018). 2I/Borisov is instead an active icy object, very similar to the comets born in our system, showing a coma and a dust tail.

2. Observations and Data Reduction

Comet 2I/Borisov was observed with the 3.58 m Telescopio Nazionale Galileo (TNG), located at the Roque de los Muchachos Observatory, La Palma, according to the Director Discretionary Time proposal. Images were acquired in the *R* band on 2019 November 3 and 23 and on 2019 December 10 and 20 with the Device Optimized for the LOw RESolution (DOLORES) instrument. DOLORES carries a 2048 × 2048 E2V-4240 CCD with a field of view of 8′.6 × 8′.6, giving a scale of 0″.252/pixel. A summary of the observations, heliocentric (r_H) and geocentric (Δ) distances to the comet, and its phase angle (ϕ) are reported in Table 1. More images have been acquired, but we have selected the four described in the table having the highest signal-to-noise ratio. Correction of the raw data for bias, overscan, and flat-field was performed using standard IRAF routines. Instrumental magnitudes were corrected for sky extinction using the TNG coefficient for La Palma.[20] Conversion to the R photometric system was performed by computing a zero-point shift from observations of the PG0918+029 standard field acquired in the same nights. The standard field was used to evaluate the accuracy of the calibration, each night better than 0.04 mag. Figure 1 shows the four images of comet 2I/Borisov obtained at the TNG telescope.

3. Probabilistic Models of the Dust Tail and Coma Brightness

The motion of the dust in the coma and in the tail depends on the β parameter, namely, the ratio between the solar radiation pressure and gravity forces (Burns et al. 1979). In the

[20] http://www.tng.iac.es/info/la_palma_sky.html

Table 1
Summary of Photometric Observations of 2I/Borisov

Date (UT)	Exp. Time (s)	Airmass	r_H (au)	Δ (au)	ϕ (°)	$Af\rho$ (m)
2019 Nov 3T05:45:20.570	60	1.52	2.15	2.39	24.49	0.59 ± 0.1
2019 Nov 23T04:57:33.391	1200	1.88	2.04	2.12	27.38	0.64 ± 0.05
2019 Dec 10T06:25:22.720	1200	1.58	2.00	1.98	28.57	0.55 ± 0.07
2019 Dec 20T06:03:08.806	1200	1.89	2.02	1.95	28.62	0.53 ± 0.05

approximation of spherical dust particles of diameter d,

$$\beta = \frac{C_{\rm pr}\, Q_{\rm pr}}{\rho_d\, d}, \tag{1}$$

where $Q_{\rm pr} \approx 1$ is the scattering efficiency for radiation pressure for millimeter-sized absorbing dust, ρ_d is the dust density, and $C_{\rm pr} = \frac{3E_{\rm Sun}}{8\pi c G M_{\rm Sun}} = 1.19\ 10^{-3}\,{\rm kg\,m^{-2}}$, with $E_{\rm Sun}$ and $M_{\rm Sun}$ the solar power and mass, c the light speed, and G the gravitational constant.

Equation (1) has been used to convert the β distribution into the dust size distribution under the assumption of a fixed value of ρ_d. However, the Rosetta dust data, on comet 67P/Churyumov–Gerasimenko (hereafter 67P), have shown that the dust density covers the widest possible range of values, from less than $1\,{\rm kg\,m^{-3}}$ up to the bulk density of sulfides, thousands of $\rm kg\,m^{-3}$ (Levasseur-Regourd et al. 2018; Güttler et al. 2019). This implies that the β distribution must be defined by a probabilistic approach. Coupled measurements of the dust mass and cross section collected by the GIADA instrument provide a probability distribution of the dust bulk density versus the logarithm of the dust size that is symmetric around the average value $\rho_d = 785^{+520}_{-115}\,{\rm kg\,m^{-3}}$ (Fulle et al. 2017). Thermophysical models of dust ejection also show that the size distribution of the ejected dust has a probability distribution versus the logarithm of the dust size that is symmetric around the average value $d_0 \approx 3$ mm (Fulle et al. 2019b, 2020). In particular, in 2014 August comet 67P ejected dust from 0.2 to 20 mm (Rotundi et al. 2015; Fulle et al. 2019b), while at perihelion from 10 μm to 0.7 m (Fulle et al. 2016, 2020). As a consequence, both the dust density and size follow a lognormal distribution. If the differential dust size distribution is a power law of the dust size with index $-\alpha$, then the β-distribution multiplied by $\beta^{\alpha-4}$ becomes proportional to the dust brightness in the case of geometric light scattering (Fulle 2004), i.e., the best approximation in the size ranges quoted above. Since the product of the lognormal distributions of two variables is a lognormal distribution of the inverse of those variables, the β distribution is

$$p(\beta) = \frac{1}{k\,\sigma}\,\beta^{\alpha-5}\exp\left[-\frac{\ln^2(\beta/\beta_0)}{2\sigma^2}\right] \tag{2}$$

$$k = \frac{1}{\sigma}\int_0^\infty \beta^{\alpha-5}\exp\left[-\frac{\ln^2(\beta/\beta_0)}{2\sigma^2}\right]d\beta, \tag{3}$$

where σ depends on the convolution of the dispersions of the dust density and sizes described above, and $\beta_0 = 5 \times 10^{-4}$ is provided by Equation (1). The Rosetta mission has shown that a dominant fraction of the dust mass falls back on the nucleus surface (Keller et al. 2017; Bertini et al. 2018; Fulle et al. 2019a), i.e., is not contributing to the coma and tail brightness. This fact has been confirmed by 67P tail models, showing that the dust size distribution above millimeter sizes is much steeper in the tail ($\alpha = 4.5$; Moreno et al. 2017) than observed by Rosetta ($\alpha = 3.5$; Fulle et al. 2016; Ott et al. 2017). The proposed probabilistic tail model is much simpler than the usual ones (Fulle 2004; Moreno et al. 2017), depending on four size-independent free parameters only, namely, the dust ejection velocity v_d at the average size of 3 mm, the dust-loss rate Q_d, the power index $-\alpha$ of the size distribution of the dust in the tail, and the dispersion σ around the average β_0 value, with a much faster best fit of the observed tails. We tested the possibility that the power index α at $\beta < \beta_0$ is different than at $\beta > \beta_0$, as found in 67P tail models (Fulle et al. 2010; Moreno et al. 2017). We found that, for $\beta > \beta_0$, the effects due to α-changes similar to those fitting the 67P tail are masked by the dominant drop of the exponential term in Equation (2), with no appreciable changes in the tail fit, which is more sensitive to changes of σ in Equation (2) than to a knee in the dust size distribution.

The proposed probabilistic approach allows us also to directly link the dust mass-loss rate Q_d (a lower limit of the dust production rate due to the significant fallout; Fulle et al. 2019a) to the quantity $Af\rho$ (A'Hearn et al. 1984; Fulle et al. 2004) measuring the dust coma brightness

$$Af\rho \approx \frac{3\,A\,Q_d}{v_d\,\rho_d\,s_0} \tag{4}$$

because, due to the probable fallout of decimeter-sized dust and the lognormal dust size distribution, both the dust mass and brightness depend mainly on the average size s_0, independent of the actual α value. With the average dust geometric albedo $A = 0.04$, Equation (4) gives

$$Q_d \approx 20\,v_d\,Af\rho, \tag{5}$$

where Q_d is in $\rm kg\,s^{-1}$ units, v_d in $\rm m\,s^{-1}$, and $Af\rho$ in m. When applied to 67P data, in 2014 August the measured values of $v_d \approx 3\,{\rm m\,s^{-1}}$ and $Af\rho \approx 0.1$ m (Rotundi et al. 2015) in Equation (5) provide $Q_d \approx 6\,{\rm kg\,s^{-1}}$, matching the dust-loss rate measured by Rosetta (Rotundi et al. 2015). At perihelion, the measured values of $v_d \approx 20\,{\rm m\,s^{-1}}$ and $Af\rho \approx 4$ m (Fulle et al. 2010, 2016) in Equation (5) provide $Q_d \approx 1.6 \times 10^3\,{\rm kg\,s^{-1}}$, close to the loss rate provided by 67P tail data (Moreno et al. 2017) and about a factor of 3 lower than the actual 67P dust production rate due to the significant perihelion fallout (Fulle et al. 2019a).

4. The 2I/Borisov Dust Tail and Coma

Comet 2I/Borisov was observed by CARA, the European network of amateur comet observers (Fulle et al. 2010), providing the time evolution of the coma brightness $Af\rho$ (Figure 2), which maintained a constant value from 2019 September to December. Our TNG observations confirm the values in Figure 2, providing

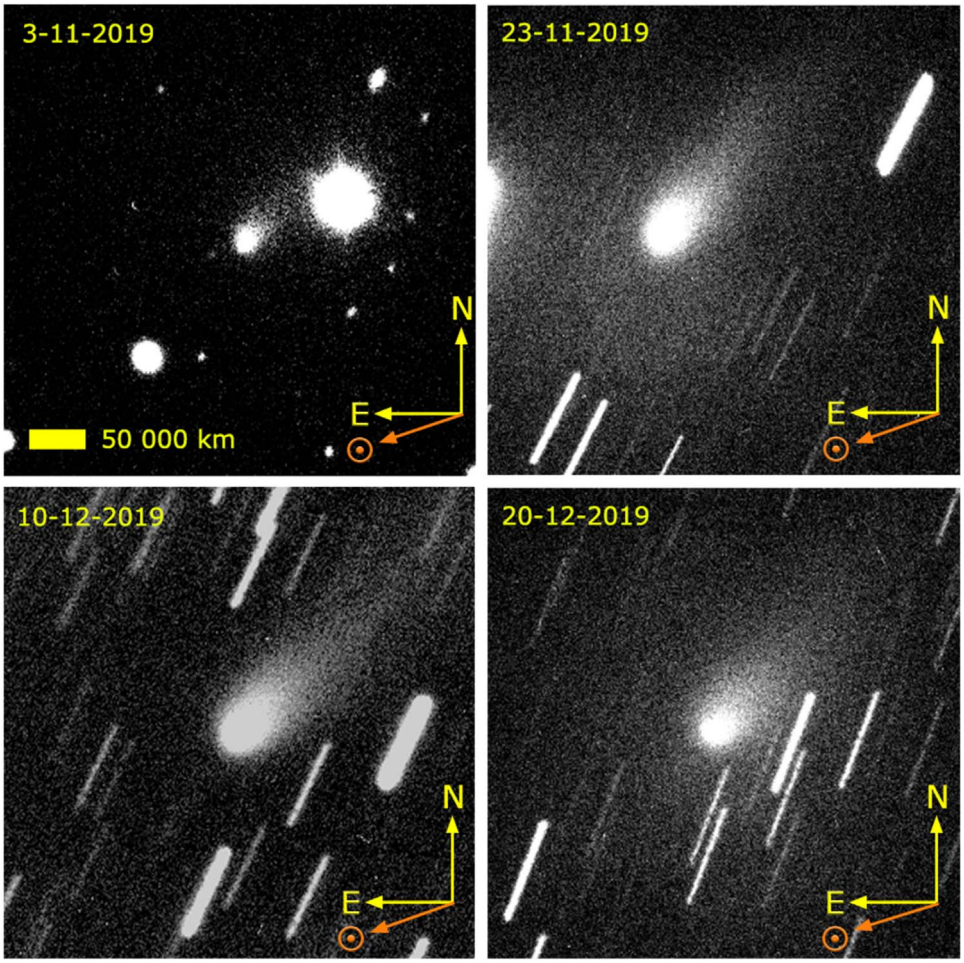

Figure 1. The four images of the comet 2I/Borisov obtained at the TNG telescope on 2019 November 3 and 23 and on 2019 December 10 and 20.

estimates with a better photometric accuracy, but the error bars are still quite large and we can only suggest a possible decrease from 2019 November to December (Table 1). The fit of the dust tail (Figure 3) was performed by a Monte Carlo numerical code adopting the β distribution given by Equation (2) with $\approx 10^8$ particles ejected isotropically (Fulle et al. 2010), providing the best-fitting parameters $v_d = 3\,\mathrm{m\,s^{-1}}$, $\sigma = 1.3$, and $\alpha = 4.5$. We assumed that the activity onset occurred at 4 au inbound, when the nucleus surface temperature overcomes 205 K, as required by the water pressure to eject dust (Fulle et al. 2020). With the value of the dust velocity provided by the tail model, Equation (5) provides $Q_d \approx 35\,\mathrm{kg\,s^{-1}}$ on 2019 November, and $Q_d \approx 30\,\mathrm{kg\,s^{-1}}$ on 2019 December. The best fit of the tail has been obtained assuming that both the loss rate and the ejection velocity are time-independent, in agreement with the $Af\rho$ values shown in Figure 2. The resulting 2I dust environment is close to that of 67P at 2 au from the Sun, suggesting that the activity of 2I and 67P may be very similar. In particular, the estimated α value suggests that dust fallout is significant on the 2I nucleus.

Given the low number of free parameters of the probabilistic tail model, it is easy to test the uniqueness of the obtained solution. In Figure 4, we compare the observed tail to the computed one changing each time only once (quoted in the figure caption for each figure panel) of the best-fit parameters. It is evident that some sets of parameters provide a tail shifted toward the antisolar direction (when too much weight is given to particles of size $<s_0$; top panels in Figure 4), whereas others

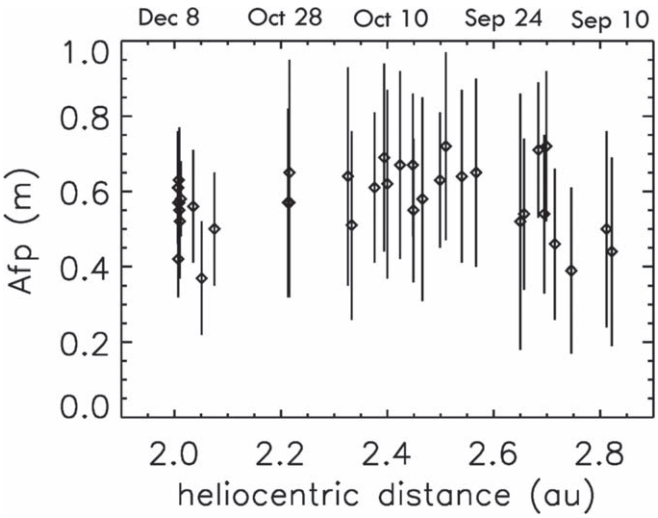

Figure 2. Coma photometry of 2I/Borisov according to the CARA network. The $Af\rho$ values have been normalized to a phase of 30°.

provide a too short tail (when too much weight is given to particles of size $>s_0$; bottom panels in Figure 4). Only the best-fit parameters provide a tail of correct orientation and length. The tail width is very sensitive to the values of the dust ejection velocity (middle panels in Figure 4), which is thus constrained with a 20% accuracy, as well as Q_d.

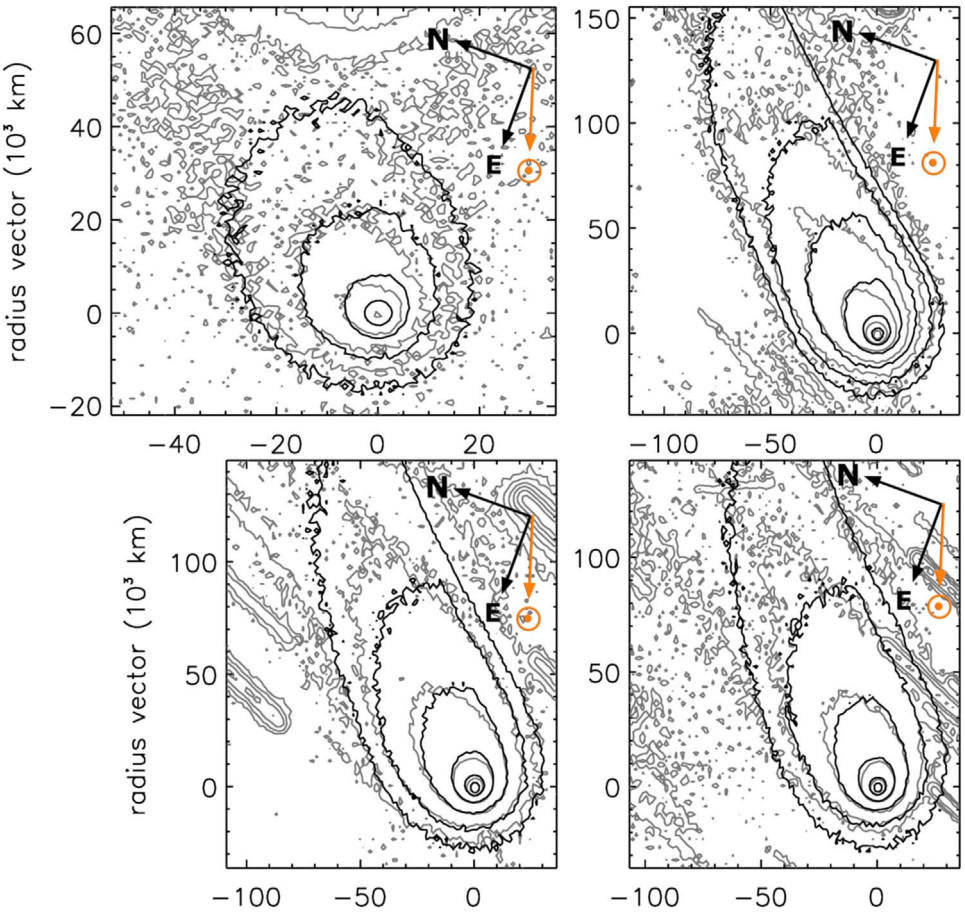

Figure 3. Computed (black isophotes) and observed (gray isophotes) dust tails on 2019 November 3 (top left panel), 2019 November 23 (top right panel), 2019 December 10 (bottom left panel), and 2019 December 20 (bottom right panel) for the best-fit parameters: $v_d = 3$ m s^{-1}, $\sigma = 1.3$, $\alpha = 4.5$, isotropic dust ejection and time-independent dust-loss rate and ejection velocity. In all the panels, the vertical axis is the antisolar direction and the innermost brightest isophote has $Af = 2 \times 10^{-7}$, with a brightness step of a factor of 3 between isophotes.

The uniqueness tests in Figure 4 show that, for dust sizes larger than 3 mm, the power index of the size distribution $\alpha \geqslant 4$ is affected by an uncertainty of ± 0.3. For dust sizes smaller than 3 mm, the α uncertainty is larger, being convoluted with that affecting σ, which depends on the dispersion of the dust bulk density and the size range of the ejected dust.

5. Conclusions

This interstellar comet has been extensively observed searching for something really new, but after a few weeks it was clear that was very similar to the Jupiter-family comets populating our solar system. The gas emissions as CN (Fitzsimmon et al. 2019) have been observed from the beginning, while other emissions have been observed a few weeks after the discovery, as C_2 (Kareta et al. 2020) and NH_2 (Bannister et al. 2020). Most of the authors point to a carbon-chain-depleted object, and this characteristic may be assumed to be less common in the Jupiter-family comets.

The good images collected at the TNG allowed us to apply our dust tail model, in the version discussed here, after the tests on the 67P and the Rosetta measurements.

The activity model, consistent with the 2I dust tail, provides a water flux from the nucleus of 8×10^{-6} kg m^{-2} s^{-1} and a nucleus erosion rate of 9 cm day^{-1} (Fulle et al. 2020). The water production rate derived from OH measurements (Xing et al. 2020) was 7×10^{26} mol s^{-1} on 2019 November 1 and 4.9×10^{26} mol s^{-1} on 2019 December 1. The ratio between these values and our water flux provides a nucleus active area of 2.5 km^2, in agreement with the estimate of 1.7 km^2 of McKay et al. (2020) providing a very similar water production rate on 2019 October 11. Assuming a nuclear size similar to 67P, having an equivalent radius of about 2 km, the percentage of the active area would be about 5%. If all the area of 2.5 km^2 ejecting water also ejects dust, the product of 2.5 km^2 times the dust bulk density times the erosion of 9 cm day^{-1} provides a dust ejection rate of 2000 kg s^{-1}, which implies a fallout of 98% when compared to the dust-loss rate derived by the tail model of 35 kg s^{-1}. Assuming this fallout value we obtain a refractory-to-water–ice mass ratio of 100, which decreases to 2 in the case of no fallout, i.e., in the case where the area ejecting dust is a factor of 50 smaller than that ejecting water. All these values are consistent with the 67P activity (Fulle et al. 2019a, 2020).

According to our model comet 2I/Borisov started its activity, based on water sublimation, at 4 au from the Sun in agreement with the suggestion of 4.5 au of Jewitt & Luu (2020). The dust-loss rate slightly decreased after the perihelion from 35 to 30 kg s^{-1}, consistent with the small decrease of the water production rate (Xing et al. 2020).

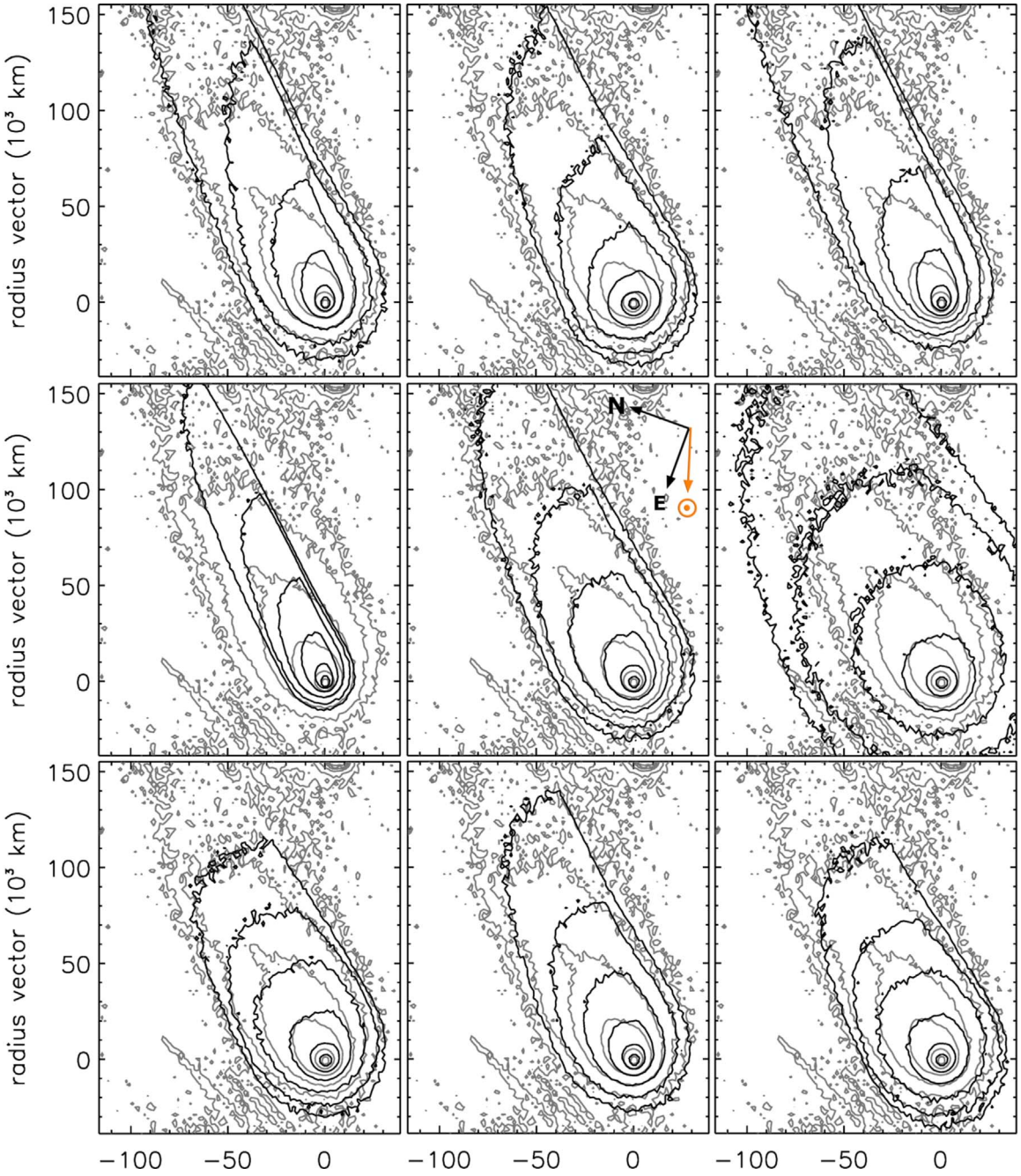

Figure 4. Test of the best-fit uniqueness by comparing the computed (black isophotes) to the observed (gray isophotes) dust tail on 2019 November 23. Each panel has one different parameter (listed hereafter) with respect to the best fit in the central panel. Top left panel: $\sigma = 1.8$. Top middle panel: Sun-faced hemispherical ejection. Top right panel: $\alpha = 5$. Middle left panel: $v_d = 1.5$ m s^{-1}. Middle right panel: $v_d = 6$ m s^{-1}. Bottom left panel: $\sigma = 0.9$. Bottom middle panel: dust-loss rate inversely dependent on the heliocentric distance. Bottom right panel: $\alpha = 4$.

We thank the Rosetta Science Ground Segment at ESAC, the Rosetta Mission Operations Centre at ESOC, and the Rosetta Project at ESTEC. Part of this research was supported by the ESA Express Procurement (EXPRO) RFP for IPL-PSS/JD/190.2016 and by the Italian Space Agency (ASI) within the ASI-INAF agreements I/032/05/0 and I/024/12/0.

Based on observations made with the Italian Telescopio Nazionale Galileo (TNG) operated on the island of La Palma by the Fundación Galileo Galilei of the INAF (Istituto Nazionale di Astrofisica) at the Spanish Observatorio del Roque de los Muchachos of the Instituto de Astrofisica de Canarias.

ORCID iDs

G. Cremonese https://orcid.org/0000-0001-9021-1140
M. Fulle https://orcid.org/0000-0001-8435-5287

References

A'Hearn, M. F., Schleicher, D. G., Millis, R. L., et al. 1984, AJ, 89, 579
Bannister, M. T., Opitom, C., Fitzsimmons, A., et al. 2020, arXiv:2001.11605
Bertini, I., La Forgia, F., Fulle, M., et al. 2018, MNRAS, 482, 2924
Burns, L. A., Lamy, P. L., & Soter, S. 1979, Icar, 40, 1
Engelhardt, T., Jedicke, R., Veres, P., et al. 2017, AJ, 153, 133
Fitzsimmon, A., Hainaut, O., Meech, K. J., et al. 2019, ApJL, 885, L9

Fulle, M. 2004, in Comets II, ed. M. C. Festou, H. U. Keller, & H. A. Weaver (Tucson, AZ: Univ. Arizona Press), 565
Fulle, M., Barbieri, C., Cremonese, G., et al. 2004, A&A, 422, 357
Fulle, M., Blum, J., Green, S., et al. 2019a, MNRAS, 482, 3326
Fulle, M., Blum, J., & Rotundi, A. 2019b, ApJL, 879, L8
Fulle, M., Blum, J., Rotundi, A., et al. 2020, MNRAS, 493, 4039
Fulle, M., Colangeli, L., Agarwal, J., et al. 2010, A&A, 522, A63
Fulle, M., Della Corte, V., Rotundi, A., et al. 2017, MNRAS, 469, S45
Fulle, M., Marzari, F., Della Corte, V., et al. 2016, ApJ, 821, 19
Güttler, C., Mannel, T., Rotundi, A., et al. 2019, A&A, 630, A24
Jewitt, D., & Luu, J. 2020, ApJL, 886, L29
Kareta, T., Andrews, J., Noonan, J. W., et al. 2020, ApJL, 889, L38
Keller, H. U., Mottola, S., Hviid, S. F., et al. 2017, MNRAS, 469, S357
Levasseur-Regourd, A.-C., Agarwal, J., Cottin, H., et al. 2018, SSRv, 214, 64
Lin, H. W., Lee, C.-H., & Gerdes, D. W. 2020, ApJL, 889, L30
McKay, A. J., Cochran, A. L., Dello Russo, N., & DiSanti, M. A. 2020, ApJL, 889, L10
Micheli, M., Farnocchia, D., Meech, K. J., et al. 2018, Natur, 559, 223
Moreno, F., Muñoz, O., Gutierrez, P. J., et al. 2017, MNRAS, 469, S186
Ott, T., Drolshagen, E., Koschny, D., et al. 2017, MNRAS, 469, S276
Rotundi, A., Sierks, H., Della Corte, V., et al. 2015, Sci, 347, aaa3905
Xing, Z., Bodewits, D., Noonan, J., & Bannister, M. T. 2020, arXiv:2001.04865